

Image-derived spectral endmembers as indicators of salinisation

R. DEHAAN and G. R. TAYLOR

School of Geology, University of New South Wales, Sydney, NSW, Australia
2052; e-mail: G.Taylor@unsw.edu.au

(Received 16 November 1999; in final form 9 August 2001)

Abstract. The objective of this research is to evaluate the utility of HyMap hyperspectral imagery for characterising and mapping irrigation-induced salinisation. Strategies for extracting and mapping spectral endmembers from HyMap imagery are assessed and a mixture-tuned matched filter approach adopted. Soil and vegetation indicators of salinisation are identified. Disturbed bare ground due to ploughing operations can be differentiated from bare ground due to salinisation. Three saline soil endmembers can be mapped and these relate well to the surface expressions of soil salinity as measured by ground geophysics. Increased salinisation is shown in the spectra of image-derived soil endmembers by the appearance of an infrared reflectance plateau between 800 nm and 1100 nm, hydrate-related absorption features at 1010 nm, 1180 nm, 1780 nm, 1950 nm and 2210 nm, the decrease in intensity (depth) of the hydroxyl absorption feature at 2200 nm and the widening of the water absorption features at 1950 nm and 1400 nm. Image-derived vegetation indicators of salinisation correspond with halophytic vegetation comprising the ‘succulent’ species of Samphire and Sea Blite and two species of native grasses. Classification of pixels according to the highest mixture-tuned matched filter score corresponds well with an independent assessment of the groundcover conditions prevailing at the time of image acquisition.

1. Introduction

1.1. *The salinity problem*

The two main styles of salinity in Australia are referred to as ‘dryland’ and ‘irrigation-induced’. While the origin of dryland salinity is hotly debated, it appears to be strongly related to both the clearing of vegetation cover and particular soil types. Irrigation salinity is more clearly related to rising water tables that can be directly attributed to additional water input to the aquifer. In irrigation areas, salt accumulation and soil degradation occur when the water table is elevated to the point where it approaches the ground surface and evaporation exceeds rainfall. Direct precipitation of evaporite minerals and destruction of primary clay minerals by interaction with salt-bearing water with which they are in disequilibrium occurs. Soil degradation due to rising saline groundwater tables is a major problem in many parts of the world. In the Murray Darling Basin of southeast Australia it is costing the nation at least US\$200 million (1987 dollars) in lost annual agricultural production (Ghassemi *et al.* 1995, p206). The major cause is poor land management, crude irrigation practices and the removal of woodlands for arable farming. The effect of

these practices has been to raise the water table to where saline water is accessible in the root zone of trees and crops. The key to successful management is the early recognition of incipient salinity, the monitoring of salt-affected land on a regular basis and the introduction of improved farming practices.

1.2. *Conventional monitoring of salinity*

Current techniques for monitoring water tables include measurement of water levels in boreholes and measurement of soil electrical properties using water extracts and ground-based geophysics. The latter technique is generally accepted as providing the best available *measurements* of soil salinity (Norman *et al.* 1989). Electrical conductivity is measured with instruments such as the EM38 (manufactured by Geonics Pty. Ltd.) and is calibrated with soil salinity measured as the conductivity of a water extract, EC1:5, (Van der Lelij and Poolman 1989). Many years of experience have established the reliability of the relationship between the traditional chemical estimate of salinity, the 1:5 extract, and the geophysical estimates. Our study is aimed at assessing the potential of HyMap to replace, or complement, the geophysical techniques as a tool for regular monitoring of soil salinity. One of the ways we measure the success of the HyMap instrument is therefore to compare the salinity maps created with those acquired by the ground geophysics. The geophysical methods are time consuming and expensive and so efforts are therefore being made to develop more cost-effective methods of mapping soil salinity. These include the use of hyperspectral imagery, airborne EM techniques (Street and Anderson 1993) and airborne radar (Taylor *et al.* 1996 a, b).

1.3. *Previous remote sensing of salinity*

Efforts to use satellite imagery, such as Landsat TM data, to map soil salinity have been largely unsuccessful. They generally rely on traditional classification techniques to monitor land cover change and are dependent on ground studies in numerous training areas (Fraser and Joseph 1998). Hick and Russell (1990) describe the use of Geoscan imagery to map soil salinity in the Western Australian wheat belt. They showed the importance of minor constituents, such as $MgCl_2$, as contributors to the spectral signature of saline soil. They also showed that vegetation vigour, as shown by near-infrared reflectances, is indicative of crop stress due to soil salinity. Taylor *et al.* (1996 a, b) show that polarimetric airborne radar can map soil dielectric properties, which are related to soil salinity. This technique, however, relies on the imagery being acquired under uniformly wet conditions to allow for the separation of moisture and salt affects. Taylor *et al.* (1994) described how principal component analysis of Geoscan imagery facilitated the qualitative mapping of salinisation at Pyramid Hill, Victoria. Bennett (1998) demonstrated that geometric unmixing techniques applied to the same data allowed for the quantitative mapping of indicators of salinisation.

The high spectral resolution of hyperspectral data (~ 10 nm) facilitates calibration of the radiance data to relative reflectances and the quantitative assessment of endmember abundance. Interpretative techniques therefore differ greatly from those traditionally applied to satellite imagery such as Landsat TM data. The research described here stems from a project having the objective of developing repeatable and accurate methods of deriving quantitative endmember abundances from hyperspectral data.

1.4. Test site description

The Tragowel Plains irrigation region is within the Murray Basin, near the town of Pyramid Hill and close to the New South Wales, Victorian border (figure 1). The Tragowel Plains Research and Demonstration Block (R and D Block) is a facility of the Victorian Department of Agriculture used to test crops and remediation measures for saline environments. This location of the R and D block is shown in all illustrated maps. Soil conductivity, as measured by ground-based geophysics, and depth to the water table are routinely monitored. The site is therefore an excellent location to test salinity mapping techniques. Agriculture involves the cultivation of various crops with annual and perennial pasture for stock under irrigation.

Soils on the R and D Block are developed upon fluvio-lacustrine clays, silts and sands of the Shepparton Formation (Macumber 1991) in excess of 100m thickness. Rising water tables have brought salt to the surface with consequent change in vegetation cover and agricultural productivity. Rising water tables first intersect the ground surface in areas of atypical low relief (Norman *et al.* 1989) which coincide with the courses of palaeo-channels. Hence the areal expression of salinised areas resemble abandoned river channels.

Geophysical surveys of the R and D Block close to the time of image acquisition have allowed us to test the validity of our results. Independent assessments of vegetation cover and species at the time of image acquisition were also made by farm personnel.

1.5. Field spectra acquisition

Spectra were collected in the field some two weeks after the image acquisition. A Fieldspec FR, manufactured by Analytical Spectral Devices of Boulder Colorado, and using the accessory reflectance probe and light source was employed. The field

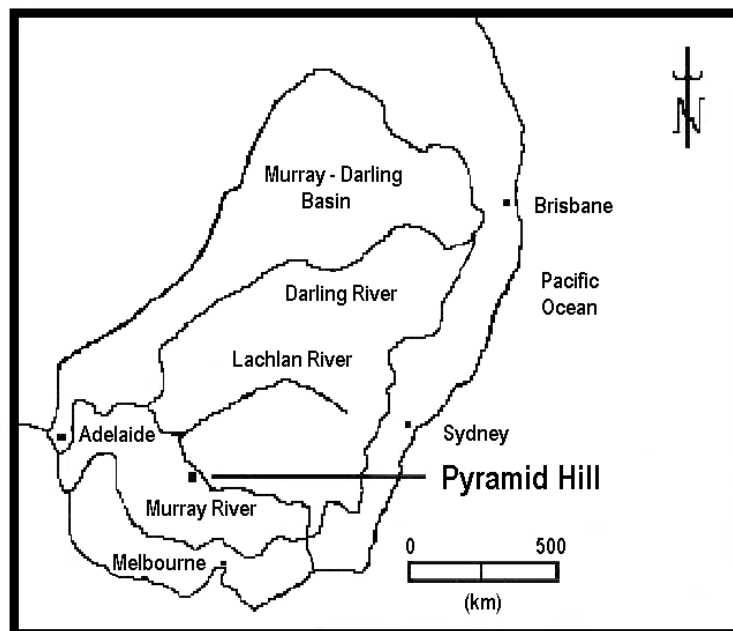


Figure 1. Location of the R and D Block, Pyramid Hill, Victoria, Australia. The boundary of the Murray Basin is shown.

of view of the instrument was restricted to 25 mm. The instrument has 2151 channels covering the spectral range 350 nm to 2500 nm and having an average bandwidth of 1 nm. Field observations were made throughout the test region but field spectra of soils and vegetation were collected only within the R and D Block. Representative sample sites were chosen by reference to soil salinity maps provided by the R and D Block personnel.

1.6. Salt composition from XRD

X-Ray Diffraction (XRD) determinations of a wide range of soil samples from the Tragowel Plains test site show that they all contain quartz, illite and kaolinite. The saline soils also contain halite and traces of anhydrite, gypsum, polyhalite, bassanite, hydroglauberite, kieserite and bloedite. Groundwater analyses provided by the Pyramid Hill Salt Company show that the ground water in the region is similar in composition to seawater and contains as major constituents dissolved sodium, potassium, magnesium, calcium, chloride and sulphate. Drake (1995) suggests that salt crusts composed of halite, gypsum, bassanite and bloedite could be expected to precipitate from such a brine. Salt crusts and soils containing hydrated chlorides and sulphates are consistent with the known composition of the groundwater.

1.7. Spectral properties of saline soils

Several papers have reviewed the spectral properties of evaporite minerals (Crowley 1991, Drake 1995). Halite (NaCl) and thenardite (Na_2SO_4) are anhydrous and show only broad features due to water within fluid inclusions or adsorbed on crystals. However, within a mineral mixture the generally high reflectivity of halite at all wavelengths can result in reflectance highs if absorption features of other constituents depress the spectra at other wavelengths. Drake (1995), quoting Hunt *et al.* (1971), describes absorption features of gypsum at around 1000 nm, 1200 nm, 1450 nm, 1600 nm, 1740 nm, 1900 nm and 2200 nm as being due to combinations of O–H stretches, H–O–H bending fundamentals and various overtones. Drake notes that the various hydrated chlorides and sulphates of sodium, potassium, calcium and magnesium share these absorption features but that variations in the way water is held in channels in crystals, and bound within the crystal lattice, cause subtle but consistent differences in the position of the absorption features. It is concluded that halite cannot be reliably identified from its spectral properties but the other possible evaporite minerals can be.

The spectra of a salt crust in a pit adjacent to the farm buildings at the R and D Block and from a salt scald are shown in figure 2(a). These spectra were collected from in-situ samples, which were damp. They show a shoulder at around 800 nm and distinct absorption features at 980 nm, 1190 nm, 1450 nm, 1775 nm, 1935 nm and 2205 nm. The water features at around 1450 nm and 1935 nm are deep and broad, consistent with the samples being damp. Spectra drawn from the USGS spectral library of halite, gypsum, bassanite and polyhalite are shown for comparison in figure 2(a).

The overall shape of spectral curves is commonly affected by non-wavelength-specific absorption and reflectance features whilst the identification of materials from their spectra is dependent on the recognition of specific absorption features. Removal of the non-wavelength-specific shape of the spectra by the continuum-removal technique allows for the specific absorption features to be more readily identified (Clark *et al.* 1990). The continuum-removed salt crust spectra are compared to an average of gypsum, bassanite and polyhalite library spectra in figure 2(b), as suggested

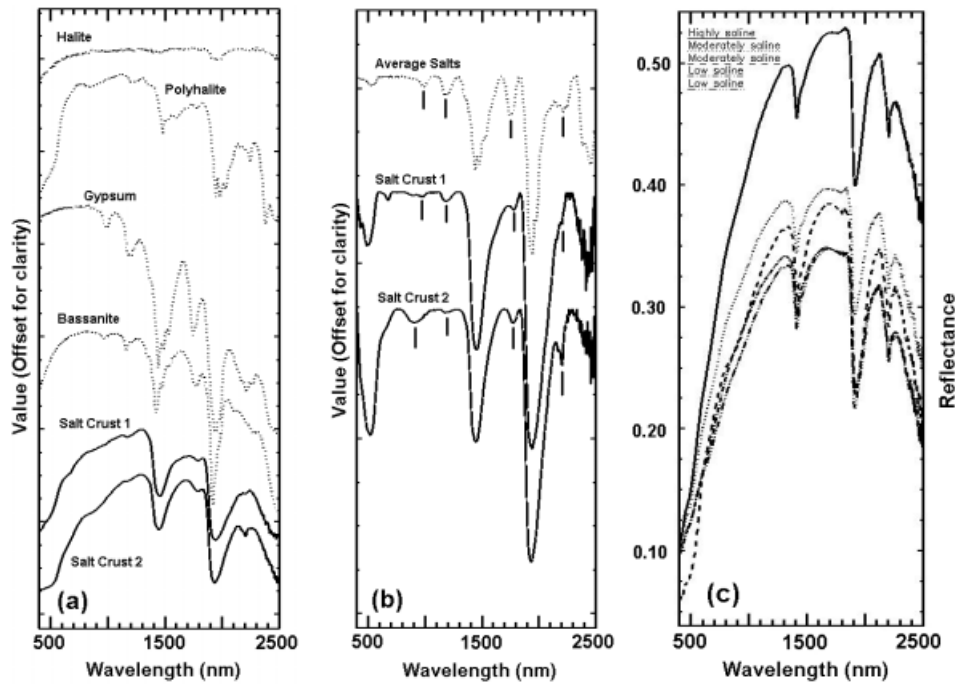


Figure 2. (a) Field and USGS library spectra for various salt crusts and minerals. (b) Continuum-removed reflectance spectra for the salt crusts and an average of the USGS library gypsum, bassanite and polyhalite and (c) field reflectance spectra for selected soils.

by the XRD analyses. The salt crust samples are contaminated with soil (especially crust 2) but their spectral features are consistent with a composition dominated by damp halite, gypsum, bassanite and polyhalite. Spectra of salt efflorescence collected in 1994 using a PIMA field spectrometer operating only in the range 1150 nm to 2500 nm, and described by Bennett (1998), show that significant amounts of gypsum were present within the efflorescence at that time. The spectra of these salt crusts therefore suggest that salt efflorescence is ephemeral in nature but that when present it is likely to be mappable from the response of the hydrated chloride and sulphate minerals.

Spectra of salinised soils collected in the field show little in the way of diagnostic absorption features. Figure 2(c) shows the field spectra of several soils possessing varying degrees of salinity as shown by their EM38 classification, their overall appearance and ability to sustain vegetation. The only significant difference in these spectra is the overall increase in reflectivity corresponding to increased salinity.

2. Hyperspectral remote sensing

2.1. The HyMap instrument

Hyperspectral imaging is defined as the acquisition of images in many registered, contiguous, spectral bands such that for each picture element a complete reflectance spectrum is derived (Goetz *et al.* 1985). Hyperspectral imagery therefore allows the user to undertake a comprehensive analysis of the composition of each pixel. The first effective hyperspectral imager was the Airborne Visible/Infrared Imaging Spectrometer (AVIRIS) which first flew in 1987. This instrument has 224 contiguous spectral bands. The Australian Mark 2 Geoscan instrument had fewer bands (46)

but approached hyperspectral imaging capabilities within some wavelength ranges. HyMap first flew in 1997 and, having 128 channels, is a true hyperspectral imager.

The HyMap Imaging System can be configured to give a variety of spectral and spatial resolutions. Band widths vary from 10 nm to 20 nm according to wavelength. Spatial resolutions from 3 to 10 m are achievable. HyMap is built by Integrated Spectronics Pty. Ltd. The instrument used in this study has 128 image channels covering the visible, near-infrared (VNIR) and the short wave infrared (SWIR). At a 5 m ground resolution the signal to noise ratio is 850 for the SWIR1 bands and 750 for the SWIR2 bands.

2.2. Interpretation strategies

The high spectral resolution of hyperspectral imagery facilitates spectral unmixing (Horwitz *et al.* 1971). A major dilemma in unmixing is whether to use endmember spectra derived from field observations or those derived from the imagery. The use of image-derived endmembers lends itself to automation and does not require the use of expensive field spectrometers or field visits. Image-derived endmembers may, however, fail to include minor terrain components that never reach abundance levels such that they dominate a single, extreme, pixel. This present contribution addresses the results of unmixing using image-derived endmembers.

Endmember abundance mapping methods include linear unmixing (Adams *et al.* 1986, Gillespie *et al.* 1990). This assumes that the reflectance at each pixel is a linear combination of each endmember present within the pixel. Unless all possible endmembers are employed the results can be spurious. Matched Filtering (MF) (Boardman *et al.* 1995) allows for the relative abundance of key endmembers to be determined without requiring a knowledge of the remaining image components. Mixture-tuned matched filtering (MTMF) (Better Solutions Consulting 1997, p 470) is a related technique that allows false positives to be identified and eliminated from the abundance result. False positives are pixels that are significantly different from the background pixels so that they are highlighted by the matched filter technique but that nevertheless do not match the signature being mapped. The technique produces an 'Infeasibility' image based on a pixel's distance from the target vector allowing 'infeasible' pixels to be identified and masked out using conventional image processing techniques. Spectral feature fitting (SFF) is another mapping method that uses a least squares technique to compare the fit of image spectra to selected reference spectra (Clark *et al.* 1990). All four methods were evaluated but the mixture-tuned results showed the best agreement with ground assessments of the degree of salinisation, due probably to the ability this technique has to eliminate false positives. Poorer results achieved by linear unmixing were probably due to our failure to correctly identify all the possible endmembers. Only the mixture-tuned matched filtering and spectral feature fitting results are described here.

Mapping endmembers based on subordinate spectral features can often only be done if a restricted wavelength range is employed. We therefore investigated whether indicators of salinity are best mapped using the entire spectral range or with restricted parts of the spectral range. We also investigated whether endmembers are best mapped using normal reflectance data or continuum-removed data.

2.3. HyMap Image acquisition and preprocessing

HyMap imagery of the Pyramid Hill region was acquired on 7 May 1999. A dark current correction was applied to the data. There seems to be little systematic variation in reflectance or spectral properties across the scene and so no correction

for across-track path-length differences ($\text{Tan } \theta$) was applied. Access to a FieldSpec FR spectrometer allowed us to collect spectra of appropriate bright and dark targets in the field. The data was then relatively calibrated by forcing the corresponding HyMap-derived spectra to fit the field spectra, using the methods of Roberts *et al.* (1986) and implemented as the Empirical Line method in the Environment for Visualizing Images (ENVI) software, (Better Solutions Consulting 1997). The targets employed were tar seal, standing water, galvanised metal roofing material and green grass. Spectra of various objects derived from the resultant, calibrated, imagery closely resemble those expected from library and field spectra. Test data was acquired with 5 m pixels for a data swath width of 512 pixels giving a ground swath width of approximately 2.5 km. A synthetic true colour composite comprised of bands 3, 9 and 15 (455, 545 and 638 nm) displayed as blue, green and red is shown in figure 3(a). This image is not registered to geographic coordinates and therefore still contains

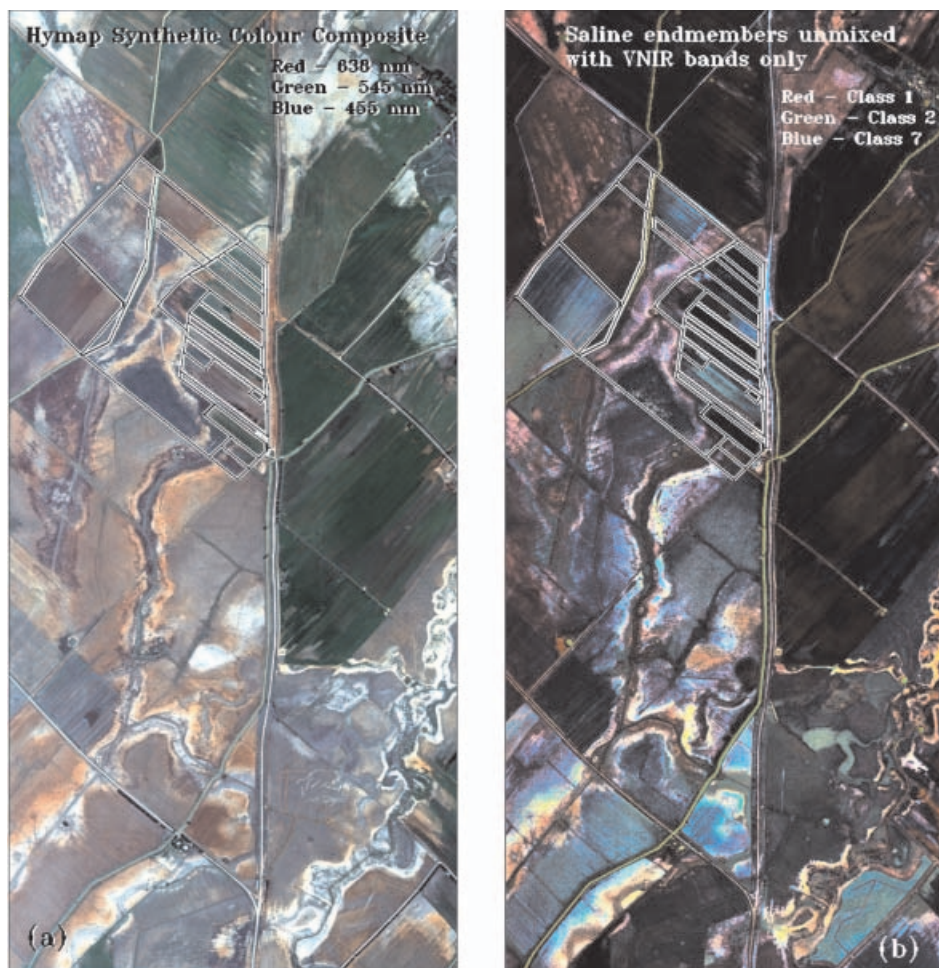


Figure 3. (a) Synthetic true colour composite of HyMap data for the Pyramid Hill test site using bands 3, 9 and 15. The extent and paddock boundaries of the R and D Block are indicated. (b) Saline soil endmembers unmixed from only the VNIR bands. Bright areas indicate that all three endmembers are abundant.

some minor geometric distortions, which do not detract from the ability to interpret the data. The image is 5 km in length from top to bottom.

2.4. Endmember identification

The Minimum Noise Transform (MNF) described by Green *et al.* (1988) was employed to both remove noise and to compress the hyperspectral data into a small number of bands. The work described in this contribution was undertaken with MNF bands derived from all 128 HyMap Bands. The MNF transformation produces principal component-like images ordered according to increasing noise content. The whole range MNF bands have information-dominated images from MNF band 1 to MNF band 20, with noise-dominated images predominating from MNF band 21 to 128. Visual inspection of the MNF bands is used to assess which bands are likely to contribute the most to the discrimination of image endmembers. It was observed that MNF band 2 was dominated by a strong shading symmetrical around the image centre line. This is thought to represent the radiance component of the across-track path-length differences and this band was therefore omitted from further processing.

Boardman (1993) has developed convex geometry-based methods for isolating extreme pixels within an image and then visualising these in a multi-dimensional display. These amounted to the effective implementation of techniques first described by Craig (1990). The most extreme pixels are identified by repeatedly projecting n-dimensional scatter plots onto a random unit vector. The extreme pixels in each projection, and the total number of times each pixel is marked as extreme, are recorded (Boardman *et al.* 1995). These extreme pixels are assumed to represent spectrally homogenous examples of the mixing endmembers. Surface materials present in sub-pixel amounts can be identified and mapped by image-derived methods only as a constituent component of a composite endmember. The MNF values of the extreme pixels are then plotted in n-dimensional space and clusters of pixels occurring at the apices of the n-dimensional data cloud classified as spectral endmembers for subsequent unmixing operations.

The Pyramid Hill data set returned over 4400 pixels as being 'hit' 18 or more times after 20,000 iterations. The n-dimensional visualiser was used to identify 26 separate endmembers or classes. The criterium for identifying these classes is that they should plot as discrete clusters of pixels in the n-dimensional plot. Identification of endmembers is an iterative process in which the extreme pixels were repeatedly displayed using as many as 7 MNF bands as visualiser dimensions. Class collapsing routines were used to aid this process. The significant endmember classes were loosely categorised as belonging to bare ground, cultivated and native vegetation groups (figure 4). No one view effectively separates all classes but each class illustrated forms a discrete cluster in particular combinations of MNF bands or views. Mean signatures in both MNF and calibrated reflectance space were extracted for each class. These were used for identification and as input to subsequent unmixing routines. No spectrally distinct class was omitted using this technique but surfaces having similar average spectral properties, due to a fortuitous combination of spectrally different materials, could be classified together. Only subsequent ground truthing could recognise when this had occurred. Three classes could not be identified as natural materials and were therefore removed from further analytical procedures.

2.5. Mapping methods

Mapping methods evaluated included spectral feature fitting, linear unmixing, spectral angle mapper, matched filtering and mixture-tuned matched filtering (ENVI manuals, Better Solutions Consulting 1997). Input to the mapping routines included

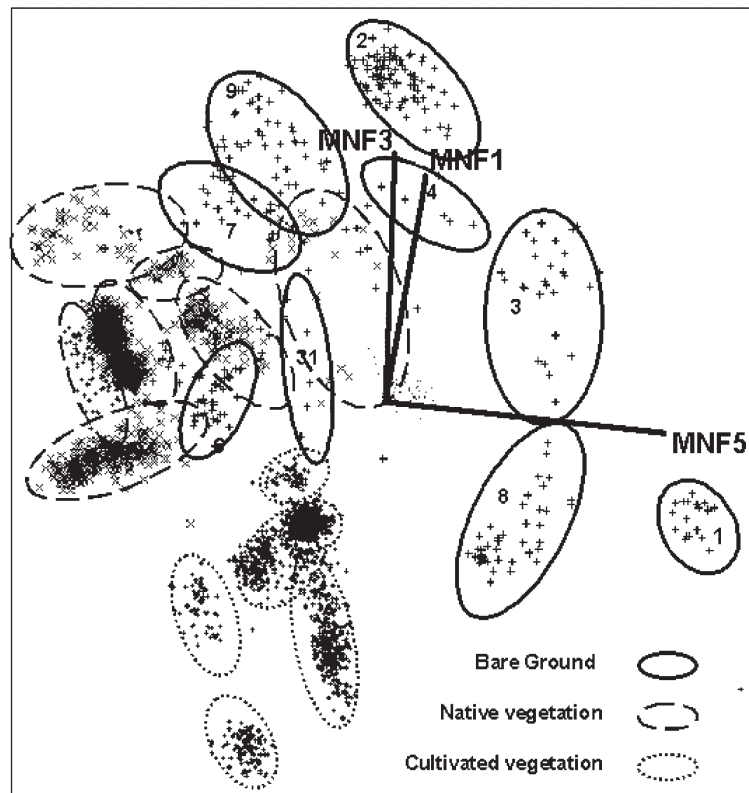


Figure 4. N-Dimensional Visualisation of extreme pixels from the Pyramid Hill HyMap scene in MNF space, MNF bands 1, 3 and 5. Bare ground, native vegetation and cultivated vegetation classes are separately illustrated and the bare ground classes are numbered.

selected high signal/low noise MNF bands, the whole-range reflectance data, selected wavelength ranges of the reflectance data and selected wavelength ranges of the continuum-removed reflectance data. The continuum-removal transformation is a way of maximising the effect of spectral features. Mapping endmember classes by any of the methods mentioned, using only the relative reflectance data, creates meaningless class maps due to the strong role played by the large water features at 1450 nm and 1950 nm. Most methods produced reconcilable class maps when continuum-removed data was used. All mapping methods were moderately successful using up to 20 MNF bands. This is because the MNF technique compresses the various sources of spectral variance present in the reflectance data into a smaller number of significant bands, making that variance more readily identified by the mapping methods used. The mixture-tuned matched filtering (MTMF) method was the most effective because of its ability to eliminate false positives from the class abundance images (Better Solutions Consulting 1997, p 470).

3. Results

3.1. Bare ground endmembers

3.1.1. Spectral properties and distribution

The 'bare ground' endmember extreme pixel clusters all plot in a discrete region of the n-dimensional space of the MNF bands, clearly separate from the vegetation,

water and manmade endmembers (figure 4). Each endmember cluster was originally assumed to be representative of a distinct soil class. However the various components of a soil such as clays, quartz, organic detritus and evaporite minerals, exist within an intimate mixture. These endmembers are likely to be locally common mixtures of these primary constituents which could form a continuum of possible compositions. For example the average reflectance spectra of bare soil endmembers 2, 4, 3 and 1, fall along a line in the n-dimensional visualiser plot shown in figure 4. Their spectra, figure 5(a), form a series which shows a systematic increase in a reflectance high at 800 nm, a decrease in the overall slope of the curve between 800 nm and 1300 nm and increased intensity and complexity in the absorption features at around 730 nm, 980 nm, 1180 nm, 1450 nm, 2000 nm, 2040 nm and 2290 nm. These absorption features are more readily seen on the continuum-removed plots illustrated in figure 6. Bare ground spectra 7, 9 and 2 also fall on a line in the n-dimensional visualiser plot. The spectra of these endmembers all possess a reflectance high at around 800 nm and a similar gradient between 800 nm and 1300 nm. However the spectrum of endmember 7 has an intense clay absorption feature at 2200 nm (figure 5(b)), which progressively

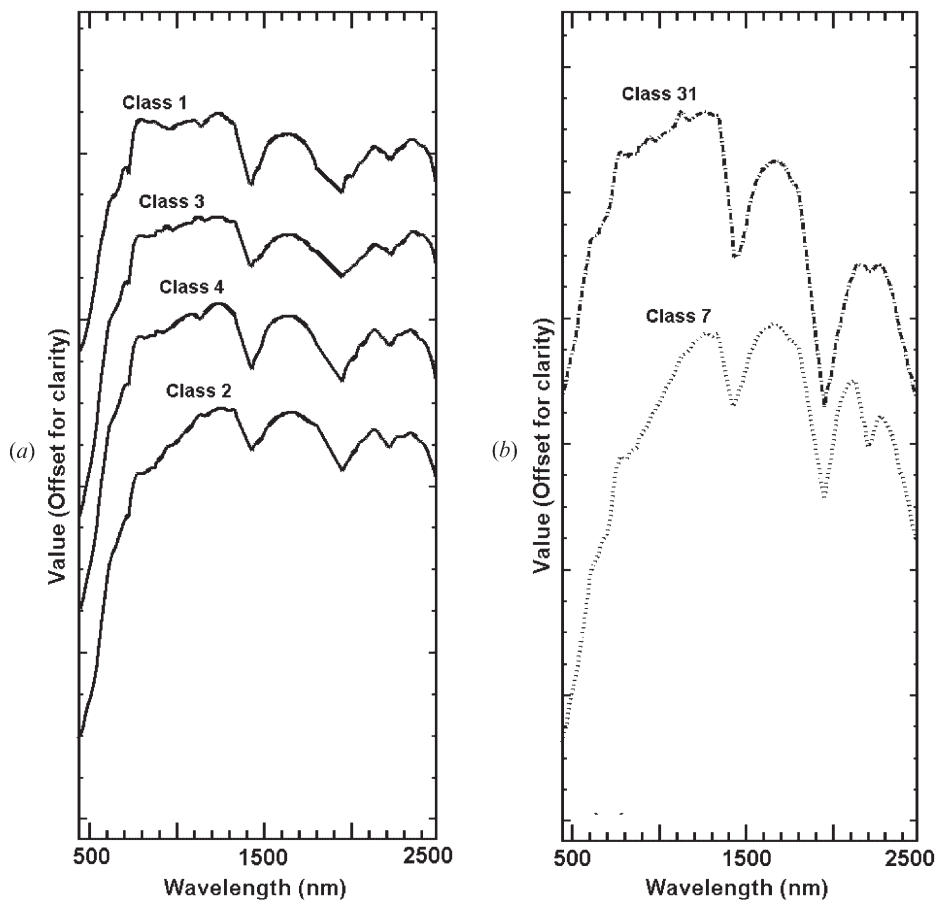


Figure 5. Reflectance spectra for HyMap image endmembers. Spectra for classes 1, 3, 4 and 2 (a) represent a related series of highly saline soils. Class 31 (b) is damp saline soil and class 7 (b) is moderately well drained saline soil within the R and D Block.

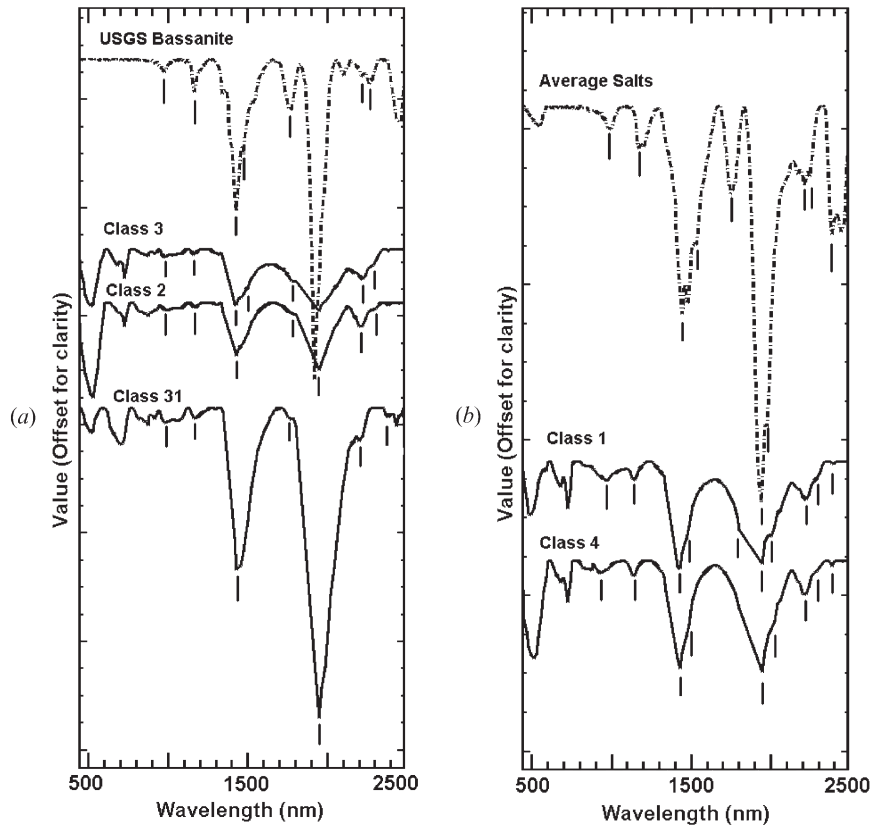


Figure 6. Continuum-removed HyMap image-derived endmember class spectra compared to (a) the continuum-removed USGS library spectra for bassanite and (b) the average spectra of USGS gypsum, polyhalite and bassanite (as indicated by XRD analyses). Significant absorption features are shown by vertical bars.

reduces in intensity in endmembers 9 and 2. These spectra do not have particular intense water features and so a high moisture content is ruled out as the cause of the reduction of the hydroxyl feature. Endmembers 9 and 2 also show a small, but significant, hydrate-related absorption feature at around 1180 nm (figure 6(a)).

The MTMF method was used to match endmember spectra to image spectra and produce class maps showing the degree of matching, or abundance, of each endmember in each image pixel (figure 7). Class 1 is coincident with the edges of the regional palaeochannels and represents the strongest surface expression of salt efflorescence. Class 2 is peripheral to class 1 and represents soils that are also salinised but that presently do not have surface salt crusts. Class 7 is more distant from the palaeochannels and coincides with areas known from the ground geophysics to be only slightly salinised. The magnitude of the scores achieved is a measure of the abundance of the component in the image pixel. On the basis of the scores achieved the most common saline soil members are 2, 9 and 7. The next most common endmembers are 4, 1 and 3. Inspection of the endmember spectra and abundance maps suggests that only endmembers 1, 2 and 7 are true endmembers and that 9, 4 and 3 represent mixtures of these true endmembers.

Non-saline soils classes include ploughed paddocks (class 12), irrigated ploughed

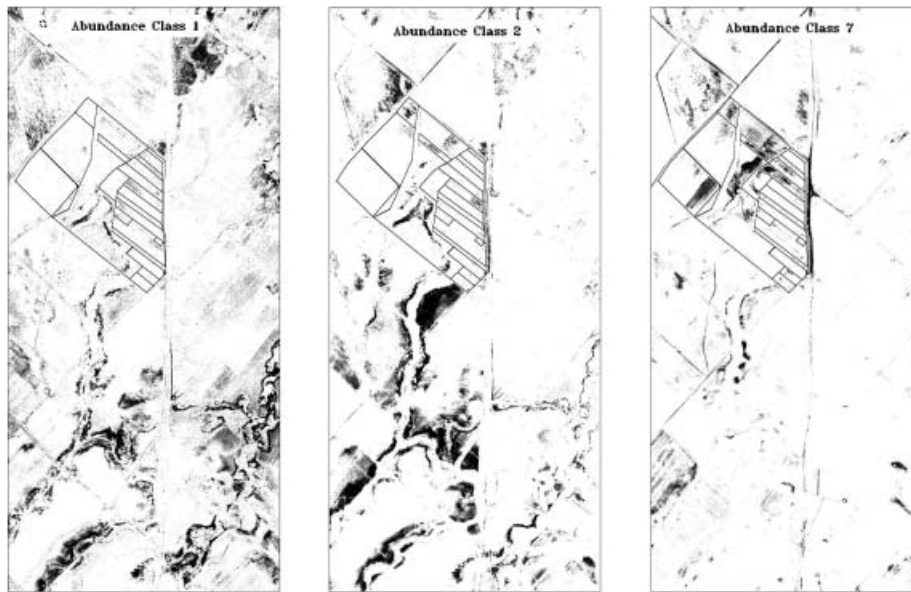


Figure 7. Abundance maps for mixture-tuned matched filter saline soil endmembers 1, 2 and 7. The boundaries of the R and D Block are shown. Abundance is directly proportional to grey-tone.

soil (class 10) and recently laid roadbase made of a goethitic/kaolinite clay foreign to the region (class 6). The abundance maps for these classes are not presented here for space reasons.

3.1.2. Interpretation

Crowley (1991) and (1993) demonstrates that infrared spectroscopy is more capable of detecting small concentrations of evaporite minerals within spectrally featureless halite than is the XRD technique. The image endmembers identified by this method are *extreme* pixels rather than *pure* pixels. They are therefore likely to comprise several, intimately intermixed, components, some of which may be present in quite small amounts. It is therefore likely that the endmember spectra are a consequence of mixing spectrally featureless halite with the spectra of soil clay minerals and minor amounts of other evaporite minerals. An accurate identification of the mineralogy of endmembers from the image-derived spectra is therefore unlikely to be possible. However some features of the endmember spectra are sufficiently distinct to suggest what components could possibly be present.

Endmembers 1, 3, 4, 2 and 31 have absorption features between 900 nm and 1200 nm that are too complex and intense to be due only to damp halite (Crowley 1993). These features resemble absorptions described by Crowley (1991) and Drake (1995), as being due to hydroxyl ions and water within the lattice of various hydrated evaporite minerals. Drake (1995) notes that the wavelength of hydrate-related absorption features varies with ionic substitution and grain size. The continuum-removed spectra, figure 6 (a), of endmembers 3, 2 and 31 resemble the spectra of USGS library mineral bassanite ($\text{CaSO}_4 \cdot \text{H}_2\text{O}$). The endmember 31 spectrum has deeper uncombined water features at 1450 nm and 1950 nm than endmembers 3 and 2 and a very small hydroxyl absorption feature at 2200 nm (figure 5(b)). This is most likely a consequence of increased moisture content in the soil (Bowers and Hanks 1965) and this class was

later recognised to be restricted to poorly drained topographic lows. Classes derived from endmembers 1 and 4 were shown to coincide with the areas of most blatant salinisation. As described previously, the composition of salt crusts from such areas is comprised of gypsum, polyhalite and bassanite, with traces of hydroglauberite, kieserite and bloedite. These are hydrated sulphates of sodium, calcium, magnesium and potassium. The image-derived spectra are therefore compared with that of the average of USGS library gypsum, polyhalite and bassanite in figure 6 (b). The spectra of these HyMap image endmembers possess the complex shoulders within the water absorption features at 1450 nm and 1950 nm that are common to several hydrated sulphates found as evaporites. However, the positions of the absorption features at around 900 nm and 1150 nm do not agree well with any of the absorption features for evaporite minerals for which we have library spectra. It is concluded that some other component, as yet unidentified, may be present.

The endmember 7 spectrum (figure 5(b)) possesses a reflectance high at 800 nm but does not show the complex, hydrate-related, absorption features within the near infrared portion of the spectrum. This spectra also possesses an intense and narrow hydroxyl absorption feature at 2200 nm, similar to that caused by the hydroxyl ions in clay minerals. This endmember occurs in areas remote from the most intense salinisation and is thought to map the most weakly salinised soils. Reduction in the intensity of the 2200 nm feature seen in the more salinised soils could be due to a loss of crystallinity following dispersion of the clay particles accompanying increased salt contents (Fraser *et al.* 1990).

The change in slope of the spectral curves between 800 nm and 1300 nm (figure 5(a)) parallels changes in soil colour from red to grey and could be due to either variations in the evaporite mineral content or to changes in the oxidation state of the iron present in the soil (Hunt and Ashley 1979). Chemical analyses to be reported in detail elsewhere show that the soils all contain similar amounts of iron, generally less than 5%, and so the colour differences and change in spectrum slope are thought to be due to variations in the evaporite mineral content. The effects of increasing salinity are therefore believed to be seen in the imagery as a reduction in intensity of the hydroxyl feature at 2200 nm (clay dispersion?), the precipitation of halite and bassanite (reflection high at 800 nm, hydrate absorption features at 980 nm and 1180 nm) and finally the formation of salt crusts containing halite and other, unidentified, evaporite minerals (very prominent reflection high at 800 nm, hydrate absorption features at 900 nm and 1150 nm, complex absorption shoulders affecting the water absorption features at 1450 nm and 1950 nm).

The suggestion that the slope of the NIR part of the spectral curve and hydrate absorption features are important contributory factors in the ability to map saline endmembers was tested by unmixing, using Spectral Feature Fitting (SFF) methods, using image data covering only the restricted spectral VISNIR range 605 nm to 1250 nm (bands 12–55). Spectra over this range were derived for the same endmembers as discussed above. Spectral features were maximised using continuum-removal methods. Almost identical endmember maps to those created by the mixture-tuned methods from the full-range MNF data were created, showing that the slope of the spectral curve and the combined water absorption features are, by themselves, sufficient to discriminate saline soils. A colour composite of saline soil classes 1, 2 and 7 obtained with this technique is presented as figure 3 (b). High abundance of all three saline endmembers, as shown by the brightest areas, coincides with the areas of greatest salinity as determined by ground geophysics (described later).

3.2. Vegetation—spectral properties and distribution

3.2.1. Halophytic vegetation

Halophytic vegetation species are useful indicators of soil salinisation. These plants have usually developed strategies for survival that give them atypical leaf and stem structures and, in some instances, unusually high moisture contents within their leaves. Halophytic plants therefore have distinctive spectral properties.

Figure 8 shows image-derived and field spectra for Pyramid Hill vegetation. Endmember 22 (figure 8(a)) is characterised by having two reflectance peaks in the visible and a distinctive slope to the infrared reflectance plateau between 1250 nm and 1400 nm. Field spectra of Samphire (*Halosarcia pergranulata*), taken close to the time of image acquisition, show the presence of three peaks in the visible range, figure 8(a) inset. The green peak predominates but there are also two small peaks in the red. Samphire is normally green but under certain seasonal or salinity conditions parts of the plant appear red. Sea Blite (*Sueda australis*), commonly known as red weed, is usually a purple/red colour and its spectra shows a strong peak in the red figure 8(a). Both plants are halophytic, often occur together at Pyramid Hill, and their unusual spectral properties are thought to be due to their fleshy, water-rich, leaves and their red colour. Endmember 22 is therefore identified as Samphire and/or Sea Blite with the Samphire predominating.

Endmembers 20 and 13 have distinctive absorption features at 2080 nm and 1720 nm (figure 7(b)) which resemble those of cotton cellulose (not illustrated), American Tumbleweed (also not illustrated) and the native grass Sea Barley Grass (*Critesion marinum*) measured at the R and D Block. The abundance map for endmember 20 resembles the known distribution of Sea Barley Grass, Hill Wallaby Grass (*Danthonia eriantha*) and Windmill Grass (*Chloris truncata*). Field spectra were not acquired for the last two species. Endmember 13 is thought to be dominated by Tall Wheat Grass (*Lophopyrum elongatum*), although other grass species are likely to be present. Endmember 15 is thought to be the halophytic species Strawberry Clover (*Trifolium fragiferum*), although again the field spectra is not available.

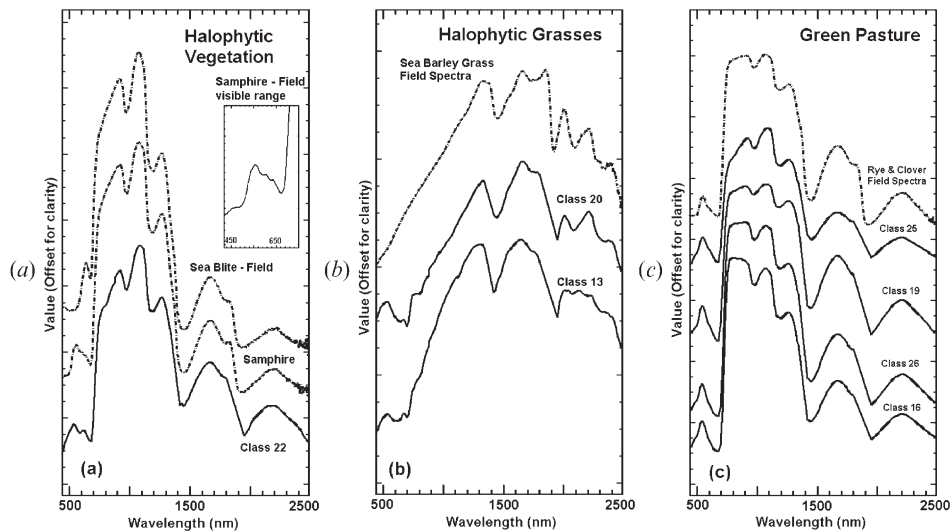


Figure 8. Image derived and field spectra for (a) Samphire and Sea Blite, (b) halophytic grasses and (c) green pasture.

Figure 9 shows the distribution of classes 22, 20 and 13. These can be reconciled with terrains dominated by Samphire and Sea Blite (22), Sea Barley Grass, Hill Wallaby Grass and Windmill Grass (20) and Tall Wheat Grass (13) respectively. The Samphire and Sea Blite member occurs where the soils are most blatantly salinised; the Sea Barley Grass, Hill Wallaby Grass and Windmill Grass occur in moderately salinised areas peripheral to the Samphire and Sea Blite; and the Tall Wheat Grass occurs in poor soils, of low salinity or in areas recovering from previously high salinity. Native grasses cannot be used as reliable indicators of salinity as their distribution is strongly affected by recent cropping and grazing practices. Samphire and Sea Blite, however, have a clear association with strongly salinised, otherwise bare, soils.

3.2.2. Cultivated vegetation

A spectra of cultivated mixed rye grass and clover pasture was collected in the field (figure 8(c)). This shows a simple green vegetation spectra with deep chlorophyll absorption features either side of the green peak at 450 nm and 680 nm, a nearly flat infrared reflectance high between 800 and 1100 nm and water absorption features at 1000 nm, 1450 nm and 1950 nm. HyMap image endmembers, classes 16, 26, 19 and 25 closely resemble this field spectra and are identified from local expert agricultural advice to be various mixes of clover, oats and ryegrass in sown pasture.

Various pasture grasses occupy all the green areas on Fig 3(a) and are apparently similar. However, the endmember maps (not illustrated) show that within paddocks different species mixes and/or different growth stages can be accurately mapped.

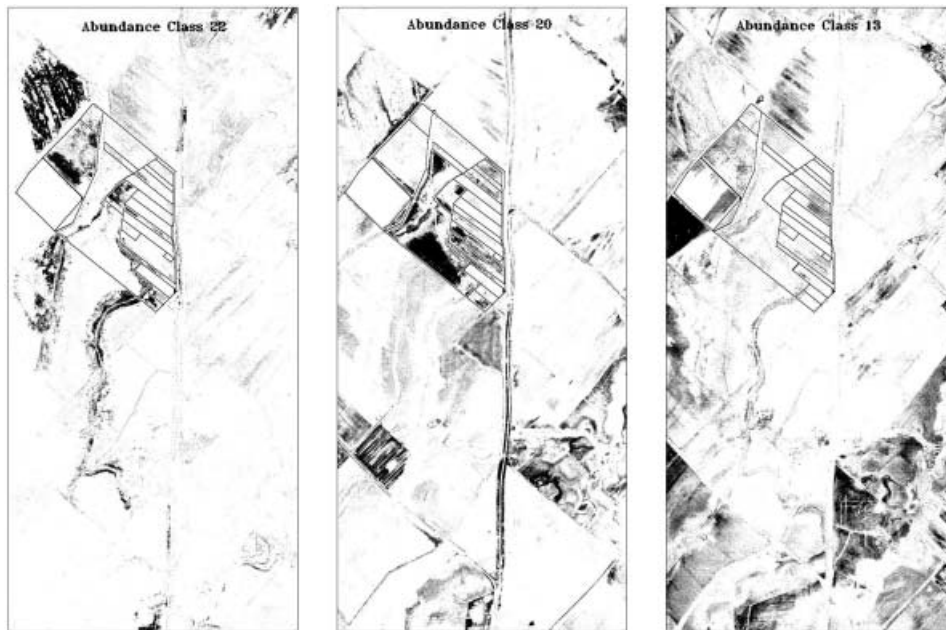


Figure 9. Abundance maps for mixture-tuned matched filter halophytic vegetation classes 22, 20 and 13. These represent the Sea Blite/Samphire endmember, the Barley Grass/Windmill Grass/Wallaby Grass endmember and the Tall Wheat Grass endmember respectively. Abundance is directly proportional to grey-tone.

4. Comparison with conventional mapping

4.1. Groundcover assessment

Endmember abundance maps are useful measures of the distribution of particular soil types, vegetation species or vegetation assemblages. However these individual maps do not give a good indication of the overall nature of a terrain as several endmembers occur within each pixel. MTF filter scores are a direct measure of endmember abundance in each pixel and can be used to determine which endmember predominates. Each pixel has therefore been classified according to its largest MTF score. The result for the area of the R and D Block is shown in figure 10. Paddock boundaries are shown and each is separately identified with an alphabetical character. Descriptions of ground cover for each paddock at the time of image acquisition are given in table 1. This information was provided by Bill Elder, Farm Manager, and was verified by ourselves soon after imaging. A simple, subjective, comparison of the actual ground cover with that identified by HyMap is provided as a 'goodness of fit' value within table 1. A correct assessment is given a score of 100%. Incorrect assessments and confused assessments are given proportionally lower scores. Both the HyMap-derived and the independent farm assessments are given in full in table 1. An average 'accuracy' of 86% is achieved. This score is excellent but it is lower than it might have been because of our failure to identify some distinctive endmembers such as soy beans, lucerne and rare eucalypts. Nevertheless we believe that the classification of terrains shown in figure 10 is a reasonably accurate reflection of the conditions prevailing at the time of image acquisition. If such maps could be generated on a multi-temporal basis they would form an excellent tool for monitoring soil condition and agricultural activity.

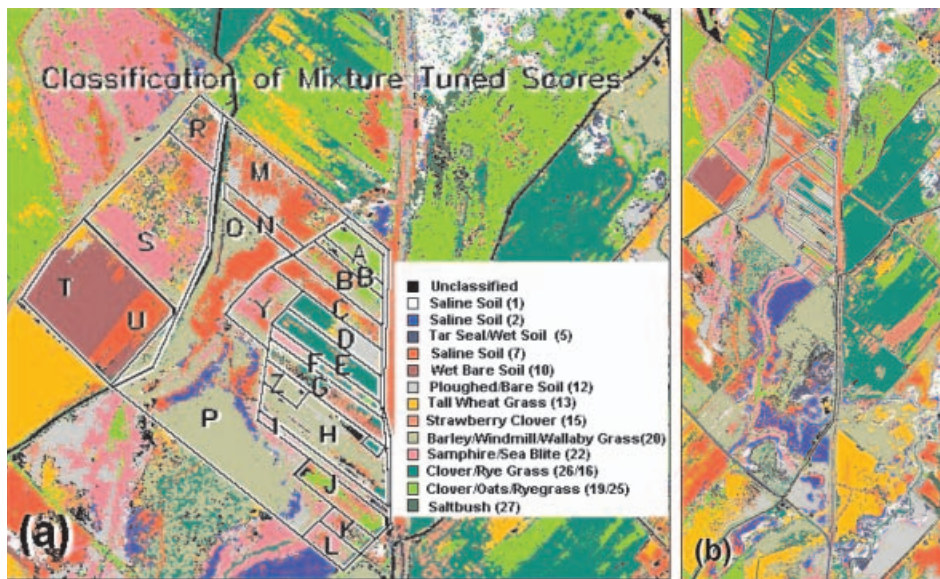


Figure 10. A simple classification of the mixture tuned filter scores showing where each class predominates. Classes have been merged to improve clarity. (a) shows the region around R and D Block with paddock identifications as used in table 1. (b) shows the classification for the same region as used in previous images and maps.

Table 1.

Key ID	Farm Description	HyMap Classifications	Fit %	Key ID	Farm Description	HyMap Classification	Fit %
A	annual pasture, clover oats and ryegrass	clover, oats and ryegrass (19/25)	100	M	part of west ploughed east is bare, saline line of eucalypts on northern boundary	west—ploughed (12) and native grasses (13/20) east—saline, mostly (7) some (1) and (2) eucalypts unclassified	80
B	annual pasture, clover oats and ryegrass, saline at west end	clover, oats and ryegrass (19/25), saline along NW edge (7)	100	N	saltbush with sparse grass understory	saline (7), native grasses (20) Sea Blite (22) and rare saltbush (27)	85
C	annual pasture, clover oats and ryegrass, saline at west end	west mostly saline (7), minor clover, oats and ryegrass in east (19/25)	80	O	highly saline Sea Blite/Samphire some Tall Wheat Grass	east—saline (7), rare (1) and (2) west—native grass (20)	80
D	west, pasture, sub-clover and ryegrass, east is ploughed	west, pasture, sub-clover and ryegrass, (26/16), east is ploughed (12)	100	P	Barley, Windmill Wallaby grass high salinity adjacent to community drain	central part—native grass 20 adjacent to drain saline (7) & (2) with some (1) and Sea Blite Samphire (22)	95
E	permanent pasture, clover ryegrass	clover/ryegrass (26/16), minor salinity in west (7)	100	R	saltbush plantation understory of grasses	saltbush (27) grasses (20/13) saline (7) Sea Blite/Samphire (22)	95
F	pasture in west, broadleaf weed and dry soy beans in east	Samphire/Sea Blite in west (22), various pasture grasses in east (26/16/19/25)	60	S	saltbush, native grasses, tall wheat grass on western fence Sea Blite/Samphire	saltbush (27) grasses (20/13) saline (7) Sea Blite/Samphire (22)	100
G	grazed lucerne plantation	some non-classified pixels, clover ryegrass (26/16) and Strawberry Clover (15)	0	T	ploughed, bare, lasered flat recently irrigated	wet bare soil (10)	100
H	fallow, bare ground, ploughed with some pasture residue, lucerne plantation at east end	some ploughed (12) rest native grasses (20) lucerne mapped as clover ryegrass (26/16)	80	U	ploughed, bare, lasered flat, moderately saline not irrigated	saline soil (7)	80
I	demo plots south of road—Sea Blite	Samphire/Sea Blite dominant (22)	100	Y	highly saline Sea Blite, native grasses, Strawberry Clover, sparse trees	saline soil (7) Sea Blite (22) native grasses (20) Strawberry Clover (15)	95
J	pasture—clover, ryegrass and Strawberry Clover	clover/oats/ryegrass (19/25) Strawberry Clover (15)	100	Z	east—Tall Wheat Grass west—saline, bare	east—Barley, Windmill, Wallaby Grass west—saline (7)	95
K & L	east—wattles, saltbush, native grasses west—saline, Sea Blite and Barley Grass	east—native grasses (20), saltbush west saline (7) Sea Blite (22)	90				

4.2. Geophysical 'measurement' of salinity

Individual saline soil endmember maps (figure 7) or composites of multiple saline soil endmember maps (figure 3(b)) give a clear indication of where salinity occurs. A subset of the multiple endmember map figure 3(b) is compared with the soil classification map obtained with ground geophysics in figure 11. The red areas in figure 11(b) are the highly saline C and D class soils as defined by the ground geophysics. The bright white areas in figure 11(a) are areas where all three saline image endmembers are abundant. Both maps show almost the same spatial distribution of high salinity classes but the HyMap-derived map is able to show greater detail because it does not rely on the coarse sampling grid of the geophysics.

5. Discussion and conclusions

Irrigation-induced soil salinity is caused by saline groundwater and elevated water tables. Optical remote sensing techniques, such as HyMap, measure the spectral properties of the top few microns of surface material. Salinity at the ground surface is a function of local topography, surface drainage, recent rainfall history, seasonal effects on vegetation growth and whether vegetation is native or cultivated. Indicators of rising salinity are therefore likely to be varied, ephemeral, and can change across paddock boundaries. This work has shown that spectral endmembers unmixed from HyMap imagery can map both soil and vegetation indicators of salinity.

As long as the soil remains undisturbed halophytic vegetation species such as Sea Blite, Samphire, Tall Wheat Grass and Barley Grass are clear indicators of soil salinity. These species can be reliably mapped with HyMap imagery. However, where the soil has been disturbed the absence of halophytes does not preclude the soil from being saline. Saline soils also give rise to areas of bare ground. Bare ground is not in itself an indicator of salinity as non-saline soils can be bare due to ploughing in preparation for crops. HyMap can, however, differentiate saline from non-saline bare ground and therefore represents a significant advance over earlier sensors in its ability to reliably map salinity. Our interim conclusions are:

1. All bare soil classes containing evaporite minerals possess the reflectance high, or shoulder, at 800 nm.
2. A decrease in slope between 800 nm and 1300 nm in spectra of saline soils is most probably due to elevated contents of evaporite minerals.

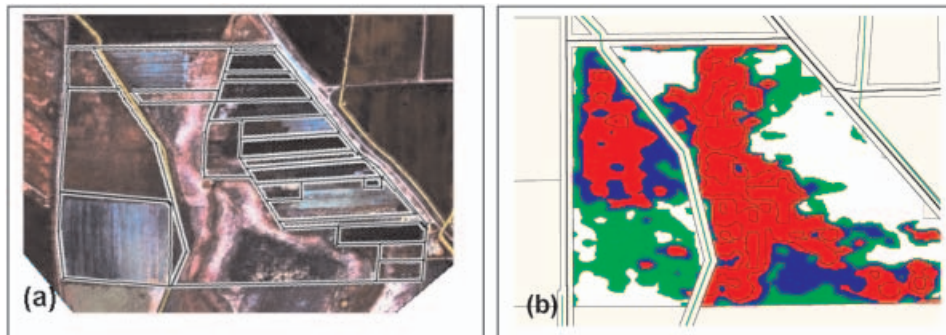


Figure 11. (a) Comparison of saline image endmember distribution derived from only the visible and NIR parts of the spectrum. This is a subset of figure 3 (b) and bright areas indicate where three saline endmembers are abundant. (b) Salinity as determined by ground geophysics. The HyMap-derived image (a) still has distortions in it due to turbulence at the time of acquisition.

3. Absorption features in the NIR part of the spectra of saline endmembers are a function of evaporite mineralogy and allow for the recognition of minerals such as gypsum, bassanite and polyhalite.
4. The increased dispersiveness of saline soils is probably accompanied by a reduction in clay crystallinity which is seen as a reduction in the depth of the hydroxyl absorption feature at 2200 nm.
5. Several categories of halophytic vegetation have distinctive spectral properties and their abundance can be mapped with HyMap imagery.
6. Abundance maps of the most saline endmember classes have a similar distribution to the map of soil salinity classes produced by ground geophysics.

This work has shown that interpretation of HyMap imagery using convex geometry methods allows for the reliable mapping of saline soils and classification of soil type and/or vegetation cover.

Acknowledgments

The authors would like to thank the staff of the Victorian Department of Agriculture Demonstration Block at Pyramid Hill for their generous assistance and cooperation. Terry and Peter Cocks of Integrated Spectronics Pty. Ltd. Are also thanked for the supply of HyMap imagery. Two anonymous reviewers made very useful suggestions that have allowed us to improve this contribution greatly.

References

- ADAMS, J. B., SMITH, M. O., and JOHNSON, P. E., 1986, Spectral mixture modelling: A new analysis of rock and soil types at the Viking Lander 1 site. *Journal of Geophysical Research*, **91**, 8098–8112.
- BENNETT, B. A., 1998, Airborne remote sensing and field spectroscopy for soil salinity mapping at Pyramid Hill, Victoria. Unpublished Masters Thesis, School of Geology, University of New South Wales, Sydney, pp.1–65.
- BETTER SOLUTIONS CONSULTING, 1997, Environment for Visualizing Images (ENVI). User guide, Version 3.0, Lafayette, Colorado, 1993–1999, 614p.
- BOARDMAN, J. W., 1993, Automating spectral unmixing of AVIRIS data using convex geometry concepts. In *Summaries of the Fourth Annual JPL Airborne Geosciences Workshop, Jet Propulsion Laboratory, Pasadena, 25–29 October 1993* (Pasadena, California: JPL Publication), 93–26, 11–14.
- BOARDMAN, J. W., KRUSE, F. A., and GREEN, R. O., 1995, Mapping target signatures via partial unmixing of AVIRIS data. In *Summaries of the Fifth JPL Airborne Earth Science Workshop* (Jet Propulsion Laboratory, Pasadena, California: JPL Publication), 95–1, 23–26.
- BOWERS, S. A., and HANKS, R. J., 1965, Reflection of radiant energy from soils. *Soil Science*, **100**, 130–138.
- CLARK, R. N., GALLAGHER, A. J., and SWAYZE, G. A., 1990, Material absorption band depth mapping of imaging spectrometer data using the complete band shape least squares algorithm simultaneously fit to multiple spectral features from multiple materials. In *Proceedings of the Third Airborne Visible/Infrared Imaging Spectrometer (AVIRIS) workshop, Jet Propulsion Laboratory, Pasadena, 4–5 June 1990* (Pasadena, California: JPL Publication), 90–54, 176–186.
- CRAIG, M. D., 1990, Unsupervised unmixing of remotely sensed images. In *Proceedings Fifth Australasian Remote Sensing Conference, Perth, Western Australia, 8–12 October 1990* (published by 5th Australian Remote Sensing Conference Incorporated, Perth), pp. 324–330.
- CROWLEY, J. K., 1991, Visible and Near-Infrared (0.4–2.5 μ m) reflectance spectra of playa evaporite minerals. *Journal of Geophysical Research*, **96**, 231–240.
- CROWLEY, J. K., 1993, Mapping playa evaporite minerals with AVIRIS data: A first report from Death Valley, California. *Remote Sensing of Environment*, **44**, 337–356.

- DRAKE, N. A., 1995, Reflectance spectra of evaporite minerals (400–2500 nm): applications for remote sensing. *International Journal of Remote Sensing*, **16**, 2555–2571.
- FRASER, D., and JOSEPH, S., 1998, Mapping soil salinity in the Murray Valley (NSW) using satellite imagery. In *Proceedings of the 9th Australasian Remote Sensing and Photogrammetry Conference, Sydney, Australia, 20–24 July 1998*. Paper published in full on CD (by Causal Productions, Sydney, Australia).
- FRASER, S. J., CAMUTI, K., HUNTINGTON, J. F., and CUFF, C., 1990, A study of the superficial clay distribution at Mount Leyshon: A comparison between XRD and spectral reflectance methods. In *Proceedings Fifth Australasian Remote Sensing Conference, Perth, Western Australia, 8–12 October 1990* (published by 5th Australian Remote Sensing Conference Incorporated, Perth), pp. 906–904.
- GHASSEMI, F., JAKEMAN, A. J., and NIX, H. A., 1995, *Salinisation of land and water resources: human causes, extent, management and case studies*, (Sydney: University of New South Wales Press).
- GILLESPIE, A. R., SMITH, M. O., ADAMS, J. B., WILLIS, S. C., FISCHER, A. F., and SABOL, D. E., 1990, Interpretation of residual images: Spectral mixture analysis of AVIRIS images, Owens Valley, California. In *Proceedings 2nd AVIRIS Workshop* (Jet Propulsion Laboratory, Pasadena, California: JPL Publication), 90–54, 243–270.
- GOETZ, A. F. H., VANE, G., SOLOMON, J. E., and ROCKS, B. N., 1985, Imaging spectrometry for earth remote sensing. *Science*, **228**, 1147–1153.
- GREEN, A. A., BERAMN, M., SWITZER, P., and CRAIG, M. D., 1988, A transformation for ordering multispectral data in terms of image quality and implications for noise removal. *IEEE Transactions on Geoscience and Remote Sensing*, **26**, 65–74.
- HICK, P. T., and RUSSELL, W. G. R., 1990, Some spectral considerations for remote sensing of soil salinity. *Australian Journal of Soil Research*, **28**, 417–431.
- HORWITZ, H. M., NALEPKA, R. F., HYDE, P. D., and MORGENSTERN, J. P., 1971, Estimating the proportions of objects within a single resolution element of a multispectral scanner. In *Proceedings, 7th International Symposium on Remote Sensing of Environment, Ann Arbor, Michigan*, ERIM, Ann Arbor, Michigan, pp. 1307–1320.
- HUNT, G. R., and ASHLEY, R. P., 1979, Spectra of altered rocks in the visible and near infrared. *Economic Geology*, **74**, 1613–1629.
- HUNT, G. R., SALISBURY, J. W., and LENHOFF, C. J., 1971, Visible and near infrared spectra of minerals and rocks, IV, Sulphides and Sulphates. *Modern Geology*, **3**, 1–14.
- MACUMBER, P. G., 1991, Interaction between groundwater and surface systems in northern Victoria. Unpublished Report, Department of Conservation and Environment, Melbourne, Victoria.
- NORMAN, C. P., LYLE, C. W., HEUPERMAN, A. F., and POULTON, D., 1989, Tragowel Plains—challenge of the plains. In Chapter 3 of Tragowel Plains Salinity Management Plan, Soil Salinity Survey, May–June 1988, Tragowel Plains Sub-regional Working Group, Victoria Department of Agriculture, Melbourne, pp. 49–89.
- ROBERTS, D. A., YAMAGUCHI, Y., and LYON, R. J. P., 1986, Comparison of various techniques for the calibration of AIS data. In *Proceedings of 2nd AIS Workshop, Pasadena, California, 6–8 May 1986* (Pasadena, CA: JPL Publication), 86–35, 21–30.
- STREET, G. J., and ANDERSON, A., 1993, Airborne electromagnetic surveys of the regolith. *Exploration Geophysics*, **24**, 795–800.
- TAYLOR, G. R., BENNETT, B. A., MAH, A. H., and HEWSON, R. D., 1994, Spectral properties of salinised land and implications for interpretation of 24 channel imaging spectrometry. In *Proceedings of the First International Remote Sensing Conference and Exhibition, Strasbourg, France, 12–15 September 1994, Strasbourg, France*, **3**, 504–513.
- TAYLOR, G. R., MAH, A. H., KRUSE, F. A., KIERYN-YOUNG, K. S., HEWSON, R. D., and BENNETT, B. A., 1996a, The extraction of soil dielectric properties from AIRSAR data. *International Journal of Remote Sensing*, **17**, 501–512.
- TAYLOR, G. R., MAH, A. H., KRUSE, F. A., KIERYN-YOUNG, K. S., HEWSON, R. D., and BENNETT, B. A., 1996b, Characterization of saline soils using airborne radar imagery. *Remote Sensing of Environment*, **57**, 127–142.
- VAN DER LELIJ, A., and POOLMAN, G., 1989, EM-38 applications in irrigated areas of southern New South Wales. Resource Monitoring Workshop, Proceedings and Abstracts, Department of Agriculture and Rural Affairs, Institute for Irrigation and Salinity Research, Tatura, Victoria, p. 13.